Scanning Microscopy

Volume 9 | Number 3 Article 4

9-20-1995

A Reflection Upon the Applicability of Electron Beam Induced Current (EBIC) as a Sensitive Microanalytical Technique (ppb range) for Silicon Materials Research

Martin Kittler
Institut fur Halbleiterphysik Frankfurt

Winfried Seifert
Institut fur Halbleiterphysik Frankfurt

Scanning Microscopy, Vol. 9, No. 3, 1995 (Pages 677-686) 0891-7035/95$5.00+.25
Scanning Microscopy International, Chicago (AMF O'Hare), IL 60666 USA

A REFLECTION UPON THE APPLICABILITY OF ELECTRON BEAM INDUCED CURRENT (EBIC) AS A SENSITIVE MICROANALYTICAL TECHNIQUE (ppb range) FOR SILICON MATERIALS RESEARCH

Martin Kittler* and Winfried Seifert

Institut für Halbleiterphysik Frankfurt (Oder) GmbH,
Walter-Korsing-Strasse 2, D-15230 Frankfurt (Oder), Germany

(Received for publication January 16, 1995 and in revised form September 20, 1995)

Abstract

This paper discusses the application of electron-beam-induced current (EBIC) technique as a tool which is able to provide at least qualitative microanalytical information not available from other techniques. Three examples are given which demonstrate a sensitivity in the parts per billion (ppb) range: temperature dependence of dislocation contrast as a fingerprint of level of metal (Cu) contamination, iron determination down to 10^{13} atoms per cm^3, and visualization of phosphorous striations in silicon grown by float-zone (FZ) method (FZ-grown Si).

Microanalytical information by EBIC is rather indirect and, usually, identification of the impurity species is not possible. Conclusions about impurity content require supplementary information and a large degree of expertise and may not be unambiguous. Nevertheless, despite these weaknesses, EBIC is considered to be a valuable tool to increase our understanding of impurity behavior, because real trace analysis methods, able to meet sensitivity and spatial requirements, are rare and utilization of indirect methods is necessary, therefore.

Key Words: Electron beam induced current, microanalysis, misfit dislocations, copper contamination, grain boundary, interstitial iron, iron-boron pairs, dopant striations, silicon.

*Address for correspondence:
Martin Kittler
Institut fur Halbleiterphysik Frankfurt (Oder) GmbH,
Walter-Korsing-Straβe 2,
D-15230 Frankfurt (Oder),
Germany

Telephone number: (49) 335-56250
FAX number: (49) 335-326195

Introduction

Due to its spatial resolution and sensitivity to electrical properties, the electron-beam-induced current (EBIC) method is a widely applied tool to study semiconductors on a microscale. Determination of minority-carrier diffusion length, lifetime, surface recombination, characterization of defects, doping inhomogeneities, and junction delineation are the main areas of application. Examples are given in numerous publications [1, 2, 4, 5, 6, 7, 18] and references therein.

In many areas of semiconductor materials research, trace analysis of impurities (e.g., metals, dopants) on the microscale and below is urgently needed. However, microanalytical techniques for this purpose are rare. In the present paper, we demonstrate that EBIC microscale data about semiconductor parameters can provide, at least qualitatively, valuable microanalytical information. Three different examples are presented: defect contrast-versus-temperature behavior, c(T), as a fingerprint for the level of copper (metal) contamination of dislocations in SiGe heterostructures, analysis of iron distribution around a grain boundary in boron-doped Si, and visualization of phosphorous striations in silicon grown by float-zone (FZ) method (FZ-grown Si).

For EBIC analysis, Schottky contacts were prepared by evaporation of either Al (p-type) or Au (n-type material), respectively. Ohmic contacts were made by rubbing Ga onto the sample. The samples were studied in a Cambridge Stereoscan S360 equipped with a Matelect ISM 5 amplifier and an Oxford cold stage.

Contrast-Versus-Temperature Behavior of Dislocations: A Fingerprint for Metal Contamination Level

Growth of Si(Ge) epilayers on (100) Si substrate results in the formation of networks of perpendicular sets of 60° misfit dislocations at the SiGe/Si interface. The density of misfit dislocations can be controlled by the Ge content and the layer thickness. For a sample with a 3 μm thick Si capping layer on top of a SiGe alloy layer

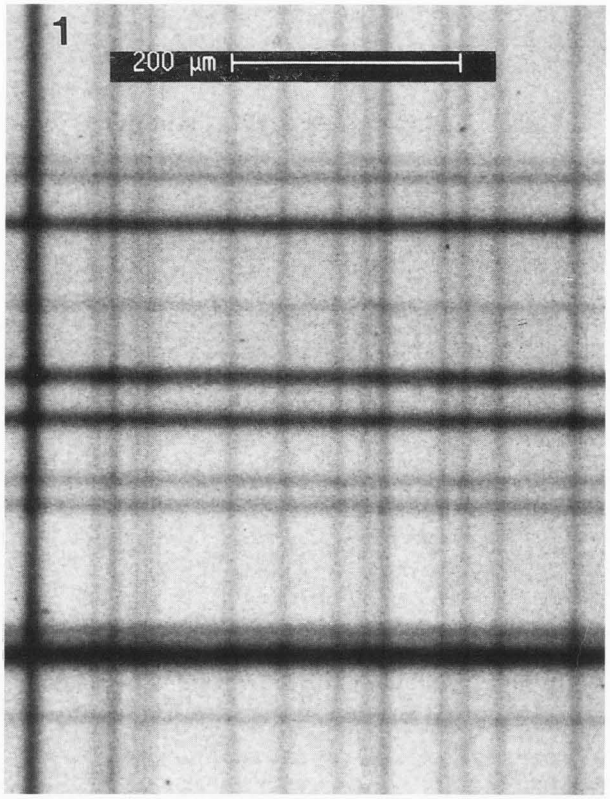

Figure 1. EBIC micrograph (30 keV) of a Si/Si(2% Ge) sample showing a network of misfit dislocations.

(2% Ge, 2 μm), the dislocation density is well suited for fundamental EBIC investigations. This possibility was demonstrated for the first time by researchers at North Carolina State University [20, 21, 22].

Misfit dislocations of this type have recently been used to study the influence of different levels of copper contamination. Cu contamination was realized in a well controlled way [3] by back-plating from a Cu salt solution and subsequent Cu drive-in at 800°C in a quartz furnace. The surface Cu concentration could be varied between 10^{11} to 10^{16} atoms/cm^2, corresponding to volume concentrations between the sub-ppb and the ppm range [3].

Figure 1 shows a typical example of misfit-dislocations related EBIC contrast features; note a network of two perpendicular sets of lines running in <110> directions. EBIC contrast values were determined from line scans across the defects at 30 keV beam energy and beam current below 0.1 nA. In **as-grown** samples, no dislocation contrast could be observed at room temperature (detection limit of our set-up better than 0.2%). Only upon cooling, the dislocations became visible, with a very weak contrast of about 0.4% at 80K [11, 13]. This temperature behavior will be denoted type II.

In **low Cu contaminated material** (ppb range), different c(T) dependencies were observed [8]. Some dislocations exhibit a positive c(T) slope denoted type-1 behavior here, with the contrast approximately proportional to $T^{1/2}$ (Fig. 2a). There are also dislocations being invisible at room temperature and showing a steep contrast increase upon cooling (Fig. 2b). This behavior is denoted type 2. In addition, some dislocations show a contrast temperature dependence of mixed type, Figure 2c. On the basis of Shockley-Read-Hall (SRH) recombination statistics, type-1 behavior is attributed to deep and type-2 to shallow levels at the dislocations [9].

In **high Cu contaminated material** (ppm range) the c(T) dependency of the majority of dislocations was observed to exhibit a positive slope (Fig. 2d). The difference, compared to type-1 dislocations, is that the contrast values for high Cu are extremely large (about one order of magnitude higher) and that the c(T) slope is weaker than $T^{1/2}$. This behavior is denoted type I.

The frequency of occurrence of a certain c(T) behavior as a function of Cu content is schematically illustrated in Figure 3. Starting from "clean" as-grown material, the type of behavior changes in the following characteristic way with increasing metal (Cu) contamination level: II → 2 (→ mixed) → 1 → I. It is noteworthy that there is no difference between n- and p-type material regarding these effects. A detailed report about the influence of the Cu contamination level on dislocation recombination behavior has been published [13].

Summarizing, one can state that the c(T) behavior of dislocations is a fingerprint characterizing the contamination level of dislocations. This was found to be an universal feature for defects in Si, being not only true for misfit dislocations contaminated with Cu reported here, but also for intra-grain dislocations in multi-crystalline Si or for dislocations formed during plastic deformation and contaminated with transition metal impurities such as Cu, Fe, and Ni [14].

Sensitive Analysis of Interaction of Iron with a Grain Boundary in Boron-Doped Silicon

Bright haloes are often found in EBIC micrographs of multi-crystalline Si. They are mostly attributed to gettering of impurities, e.g., iron [7, 25]. However, these getter zones have only been investigated qualitatively so far. Here, we present a quantitative analysis of iron gettering by a grain boundary (GB) based on the essential methodological advantages of iron. Namely, in B-doped silicon, Fe is known to form **FeB pairs** (shallow donor at E_v + 0.1 eV) which are of low recombination activity at room temperature. These pairs can be destroyed easily by carrier injection or annealing, leaving iron in the form of **interstitial iron**, Fe_i (deep donor at E_v + 0.4 eV), which is an efficient recombination

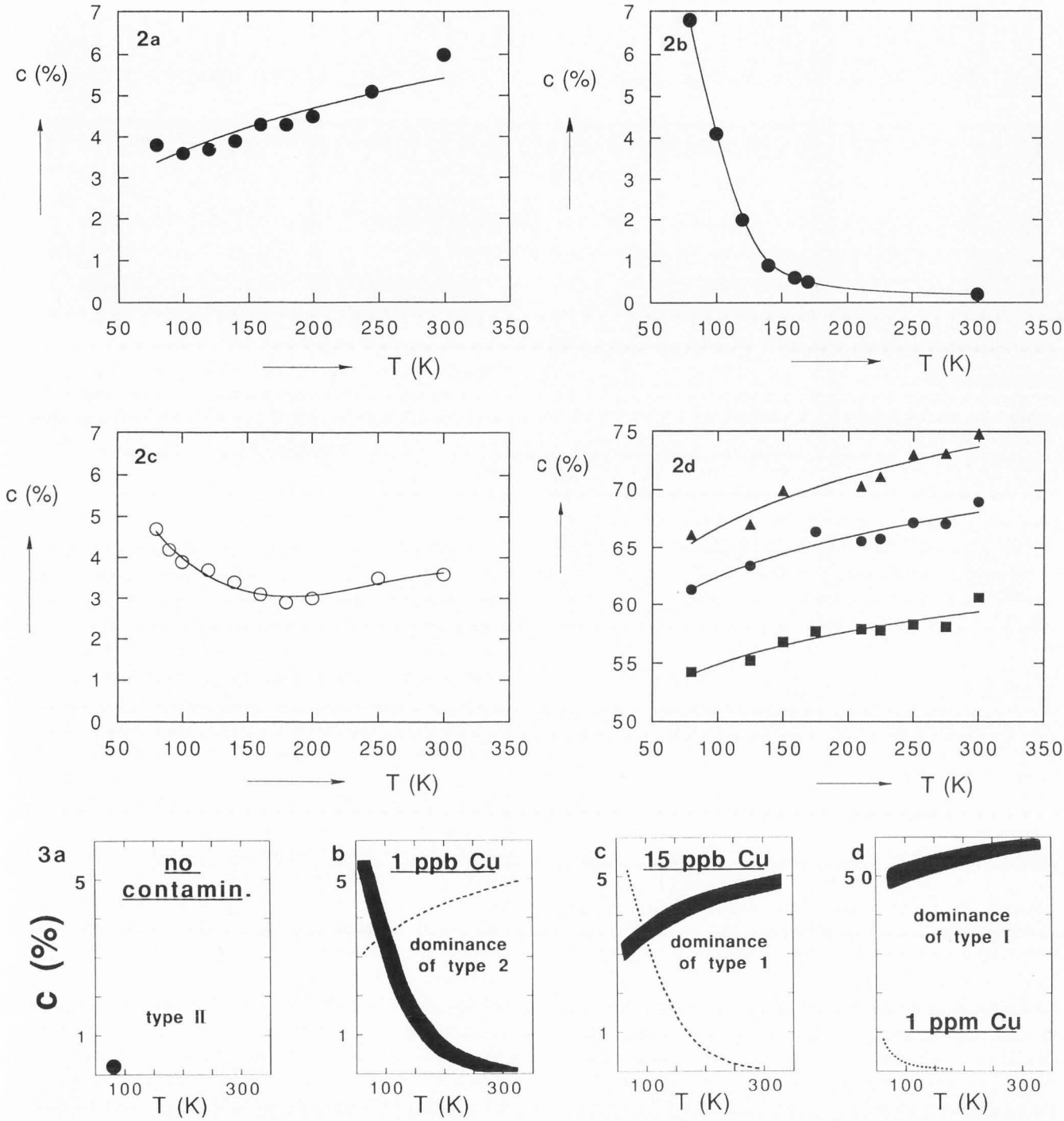

Figure 2. Different temperature behavior of EBIC recombination contrast c(T) as observed between 80 and 300 K for misfit dislocations in low Cu contaminated material (**a**, **b**, and **c**) and high Cu contaminated material (**d**). Contrast visible in the whole temperature range, positive slope of c(T): type-1 behavior (**a**); no contrast at room temperature but visible contrast upon cooling, negative slope of c(T): type-2 behavior (**b**); mixed character of type-1 and -2 behavior (**c**); much higher contrast as type-1 in the whole temperature range: type-I (**d**).

Figure 3. Schematic illustration of dominant types of c(T) behavior in dependence on Cu content. No contamination: type-II behavior (**a**); 1 ppb Cu: dominance of type-2 behavior, only a few dislocations show type 1 (**b**); 15 ppb Cu: dominance of type-1 behavior, only a few dislocations show type 2 (**c**); and 1 ppm Cu: dominance of type-I behavior, only a few dislocations show type 2 (**d**).

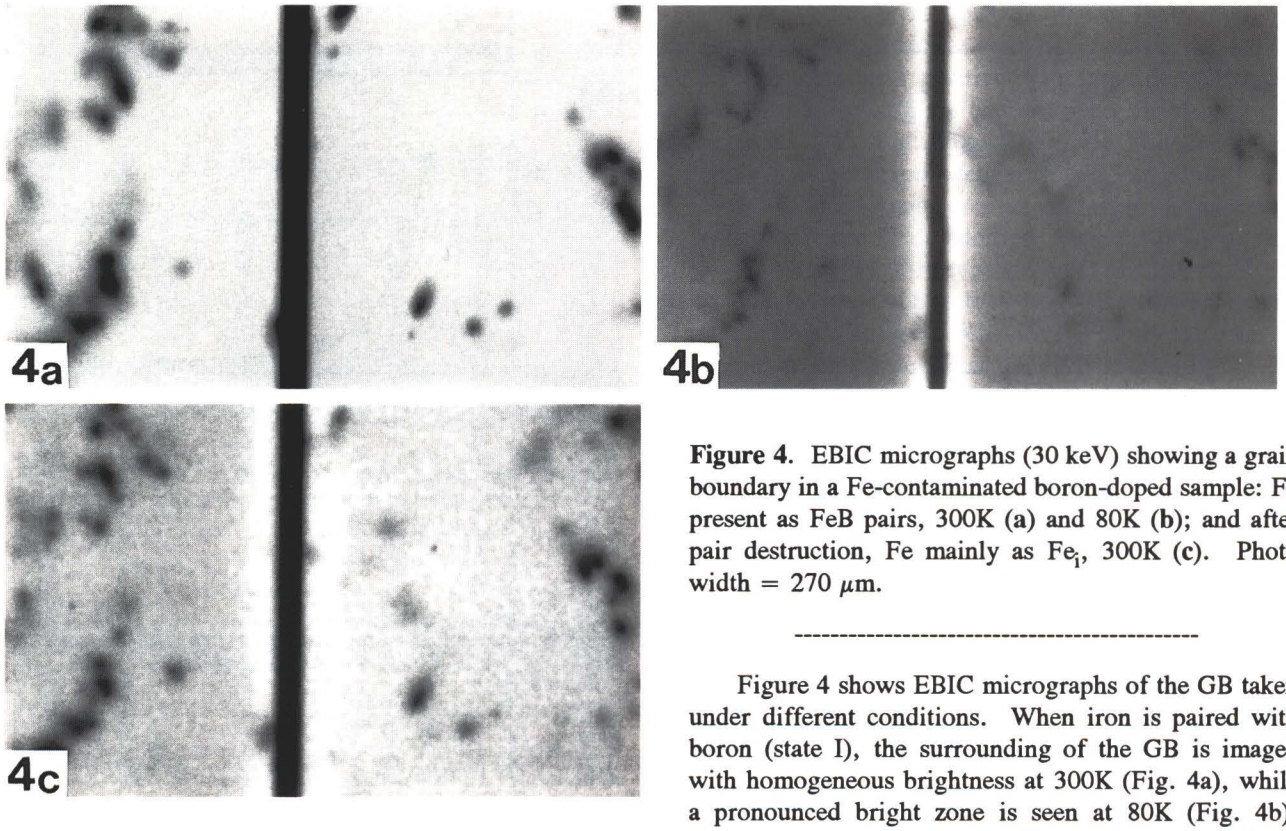

Figure 4. EBIC micrographs (30 keV) showing a grain boundary in a Fe-contaminated boron-doped sample: Fe present as FeB pairs, 300K (a) and 80K (b); and after pair destruction, Fe mainly as Fe_i, 300K (c). Photo width = 270 μm.

---

center at 300K unlike FeB. Thus, measuring the minority-carrier diffusion length before (L_I) and after (L_{II}) pair destruction allows one to estimate the interstitial iron concentration using

$$\{Fe_i\} \simeq \{(L_{II}^{-2} - L_I^{-2})\, D / \sigma V_{th}\} \qquad (1),$$

where D is electron diffusivity; σ is the electron capture cross-section of Fe_i (2×10^{-14} cm^2 [19]) and V_{th} is thermal velocity of electrons. This was demonstrated for the first time in 1986 [10], where we could show that EBIC allows an estimate of the iron content in the 10^{13} cm^{-3} range on the microscale. The principle of this technique is now widely used in semiconductor industry for iron detection in Si with a smaller spatial resolution but higher sensitivity, where optical methods are used for the required diffusion-length/recombination lifetime determination [26].

Results of an investigation of a Wacker SILSO sample (boron concentration 4×10^{15} cm^{-3}; Wacker GmbH, Burghausen, Germany) containing a high-angle GB are briefly discussed. Iron was introduced by evaporation of the sample back side and subsequent annealing at 1000°C for 15 minutes followed by quenching. The sample was studied in two different states: State I with iron present as FeB pairs and state II after destruction of the pairs by forward biasing of the Schottky junction [10], i.e., with about 80% of iron in the Fe_i form.

Figure 4 shows EBIC micrographs of the GB taken under different conditions. When iron is paired with boron (state I), the surrounding of the GB is imaged with homogeneous brightness at 300K (Fig. 4a), while a pronounced bright zone is seen at 80K (Fig. 4b). After pair destruction (state II), a slight zone of enhanced brightness becomes visible near the GB already at 300K (Fig. 4c). The relatively small width of the bright getter zone around the GB makes both direct DL determination in the getter zone and evaluation of the GB recombination velocity from contrast measurements impractical. Therefore, a Monte-Carlo model presented recently by Stemmer [24] was used to deduce these parameters of interest from profiles of charge-collection efficiency η, recorded across the GB. In Figure 5a, such experimental data are presented together with fitted profiles, while Figure 5b shows the corresponding DL values and the product of GB recombination velocity V_s and diffusivity D (1.2×10^7 cm^{3}s^{-2} at the top). A stepwise DL distribution was assumed for simplicity. After pair destruction, a clear increase of the DL is established in 20 μm wide zones on both sides of the GB. It is also found that the GB recombination velocity is not affected by the pair destruction treatment within the accuracy of experimental data and model.

The DL profiles (Fig. 5b) extracted from the EBIC efficiency profiles were converted into concentrations of the solved iron using:

$$\{Fe\} \simeq \{Fe_i\} / 0.8 \simeq \{1.2 \times 10^{16} (L_{II}^{-2} - L_I^{-2})\ \text{cm}^{-3}\} \qquad (2)$$

where L_I and L_{II} given in μm.

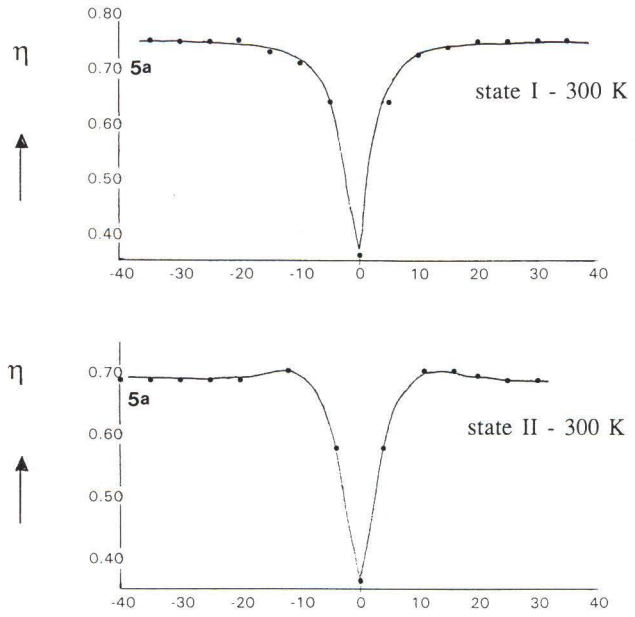

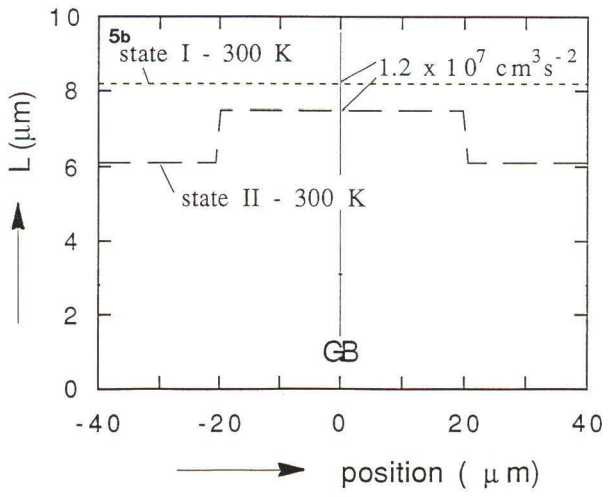

Figure 5. EBIC profiles at the grain boundary (GB): (a) Theoretical profiles of charge collection efficiency η versus beam position (————) and experimental data points (•). **State I**: 300K represents the situation with FeB pairs; and **State II**: 300K, the situation after pair destruction/formation of Fe_i. For calculation of the theoretic profiles, the corresponding diffusion-length profiles and recombination velocity, shown in (Fig. 5b), were used. (b) Diffusion-length profiles and V_s x D product (a GB recombination velocity of $V_s = 5 \times 10^5$ cm s^{-1} is estimated when D = 25 cm^2 s^{-1} is assumed) allowing the best fit to the experimental data shown in (a).

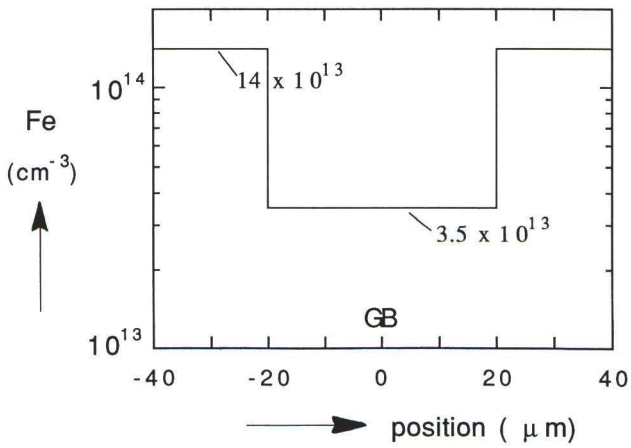

Figure 6. Profile of iron concentration, deduced from the diffusion-length profiles in Figure 5b, pointing to gettering of about 4 x 10^{11} iron atoms per cm^2 at the GB.

The iron profile is shown in Figure 6 with 0.35 x 10^{14} cm^{-3} iron in the getter zone and 1.4 x 10^{14} cm^{-3} far from the GB. The iron value far from the GB corresponds to deep level transient spectroscopy (DLTS) data (about 2 x 10^{14} cm^{-3}). The pronounced iron depletion around the GB indicates a gettering of 4 x 10^{11} cm^{-2} iron atoms to the GB. A detailed analysis and discussion of EBIC data on GB iron gettering, taking into account also the temperature dependence of recombination properties was recently published [12]. The results emphasize the high sensitivity of EBIC for recording iron distributions in B-doped Si, including interaction of Fe with extended defects. The detection limit of this technique is in the range of {Fe} $\leq 10^{13}$ cm^{-3} on the scale of some μm. That means that for an information volume of about 10^3 μm^3, the detection limit is about 10^4 iron atoms.

Detection of Phosphorous Striations in FZ-Grown Silicon

Impurities with segregation coefficient differing from unity are inhomogeneously incorporated into growing crystals, giving rise to so-called growth striations [23]. Here, we describe the investigation of dopant striations in phosphorous-doped (10^{14} cm^{-3}) FZ-grown silicon crystal.

An EBIC panorama taken from a wafer of this crystal at E_o = 10 keV is given in Figure 7. Curved contrast features due to striations are clearly visible. Figure 8 shows micrographs of the same sample imaged with 40 keV (Fig. 8a) and 10 keV (Fig. 8b), demonstrating contrast inversion of the striations. The micrographs taken at low beam energy show much more pronounced contrasts than the high beam energy images.

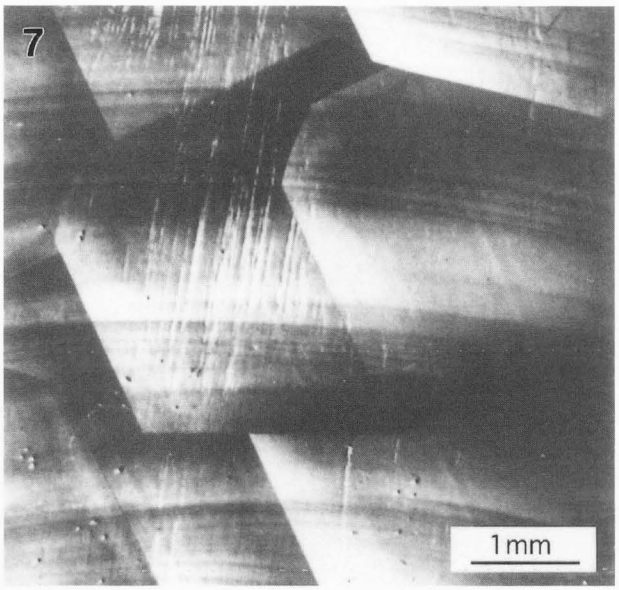

Figure 7. Phosphorous striations in FZ-grown silicon imaged by EBIC at 10 keV.

If these striated features are related to microdefects, (microdefects are well-known to act as recombination sites with dark EBIC contrast), no contrast inversion appears and, furthermore, for low beam energy, smaller contrast values would be expected. Indeed, microdefects could not be revealed by preferential etching.

Thus, the observed effects are believed to be due to modulation of depletion layer width, w, and electrical field, E, of the collecting Schottky barrier (see also [16]) by the dopant/phosphorous inhomogeneities according to:

$$W \alpha 1/\sqrt{N} \quad \text{and} \quad E \alpha \sqrt{N} \qquad (3)$$

where N is the net doping concentration. This is briefly explained in Figure 9. In Figure 9a, the situation is shown schematically for a large beam energy where the generation volume of the electron-hole pairs extends to the neutral semiconductor. Assuming complete charge collection in the depletion layer but collection losses in the neutral material, resulting from recombination of minority carriers there, a higher signal is expected from regions with a smaller dopant concentration.

Figure 9b illustrates the situation for a small beam energy where the generation region is located in the depletion layer. The schematic distribution of the electrical field in the Schottky junction is sketched, too. Assuming that, at sufficiently high excess carrier density, larger collection losses appear in regions of lower

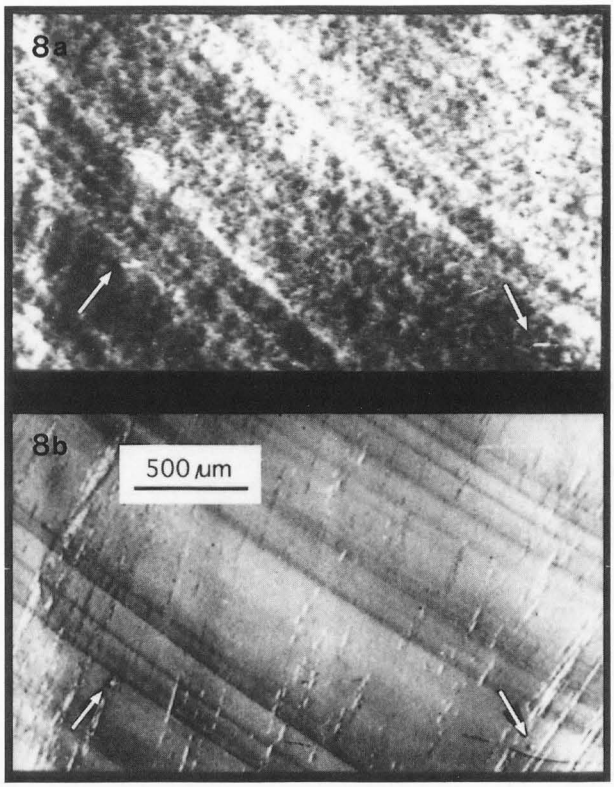

Figure 8. EBIC micrographs of growth striations taken at 40 keV (a) and 10 keV (b). Note the contrast inversion. The arrows mark identical sample positions.

---

field [17], the lower-doped region results in a lower signal, which is just the opposite to what is observed at high energy. The type of contrast inversion discussed is considered as evidence of doping inhomogeneities, so the contrast pattern in Figure 8 reflect the distribution of phosphorous.

It is worth noting that spreading resistance measurements did not reveal the striation-related resistivity/ dopant inhomogeneities in the material. This points to the high sensitivity of EBIC to detect spatial inhomogeneities of dopants, especially if the mean dopant concentration is small.

A quantitative determination of the dopant variation in this material seems to be not possible, however. At high beam energy, where the effect could be modelled in principle, the dopant-related contrasts are too small for quantification, because in the neutral material, the recombination is too small (the diffusion-length is too large). On the other side, at low beam energy dopant-related contrasts are really strong, but, to our knowledge, no model is available that would allow the quantification of the EBIC in the depletion layer as a function of electrical field and excess carrier concentration.

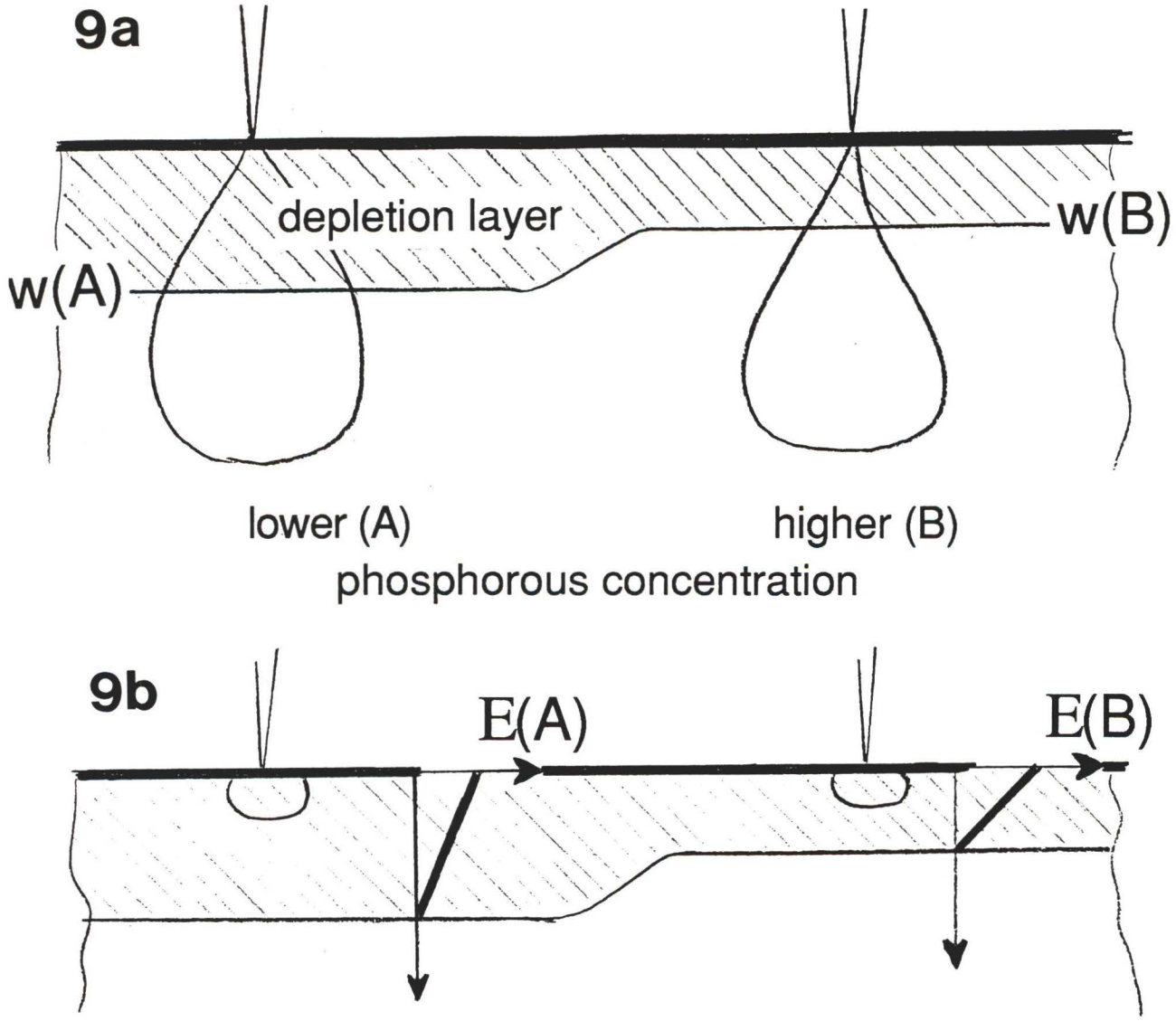

Figure 9. Schematic illustration of charge collection in material with dopant inhomogeneities at high beam energy (**a**) and low beam energy (**b**). At high beam energy, a higher EBIC signal is expected for region A, exhibiting a larger depletion layer width than region B ($W_A > W_B$). At low beam energy, a higher EBIC signal is expected for region B, exhibiting a stronger electrical field ($E_B > E_A$) in the Schottky junction than region A.

Conclusions

The examples presented demonstrate that EBIC is sensitive to impurity concentrations down to the ppb range. Together with the small volume probed by the electron beam, this offers an opportunity to obtain, at least qualitatively, microanalytical information on a microscale. Of course, microanalytical information by EBIC is rather indirect and, usually, identification of the impurity species is not possible. Conclusions about impurity content require supplementary information and a large degree of expertise and may not be unambiguous. Nevertheless, despite all these weaknesses, EBIC is considered to be a valuable tool to increase our understanding of impurity behavior, because real trace analysis methods, able to meet sensitivity and spatial requirements, are rare and utilization of indirect methods is necessary, therefore.

The high sensitivity observed in EBIC is due to electrical effects caused by impurities. Techniques such as cathodoluminescence (CL) and scanning DLTS (S-DLTS) have a similar background and allow micro-

analysis as well, in particular, they are spectroscopical methods and so, in principle, are capable to identify species. However, CL is not very suited for Si (as an indirect semiconductor material) and S-DLTS is a technique much more difficult than EBIC and still development regaring application to silicon [15].

Acknowledgments

The authors thank Z.J. Radzimski for SiGe samples, V. Higgs for copper contamination, J. Palm for iron contaminated multi-crystalline material, M. Stemmer for Monte-Carlo simulations, J. Lärz for help with EBIC investigations, K. Tittelbach-Helmrich for DLTS studies and P. Gaworzewski for spreading resistance measurements. Further, the authors acknowledge support by the Bundesministerium für Bildung, Wissenschaft, Forschung und Technologie, Bonn, under contract number 0329107.

References

[1] Donolato C (1979) Contrast formation in the SEM charge-collection images of semiconductor defects. Scanning Electron Microscopy, **1979**: I; 257-274.

[2] Hanoka JI, Bell RO (1981) Electron-beam-induced currents in semiconductors. Ann Rev Mater Sci **11**, 353-380.

[3] Higgs V, Goulding M, Brinklow A, Kightley P (1992) Characterization of epitaxial and oxidation-induced stacking faults in silicon: The influence of transition-metal contamination. Appl Phys Lett **60**: 1369-1371.

[4] Holt DB, Joy DC (1989) SEM Microcharacterization of Semiconductors. Academic Press, London, U.K. pp. 241-338.

[5] Holt DB, Lesniak M (1985) Recent developments in electrical microcharacterization using the charge collection mode of the scanning electron microscope. Scanning Electron Microscopy **1985**; I: 67-86.

[6] Jakubowicz A (1987) Theory of electron beam induced current and cathodoluminescence contrasts from structural defects of semiconductor crystals; steady-state and time-resolved problems. Scanning Microsc **1**: 515-533.

[7] Kittler M, Seifert W (1992) On the origin of electron-beam-induced-current contrast of extended defects in silicon. Scanning Microsc **6**: 979-991.

[8] Kittler M, Seifert W (1993) Two classes of defect recombination behaviour in silicon as studied by SEM-EBIC. Scanning **15**: 316-321.

[9] Kittler M, Seifert W (1994) Two types of electron-beam-induced current behaviour of misfit dislocations in Si(Ge): Experimental observations and modelling. Mater Sci Eng **B24**: 78-81.

[10] Kittler M, Seifert W, Schmalz K, Tittelbach-Helmrich K (1986) Comparison of EBIC and DLTS measurements on boron-doped CZ silicon contaminated with iron. phys stat sol (a) **96**: K133-K137.

[11] Kittler M, Seifert W, Higgs V (1993) Recombination activity of misfit dislocations in silicon. phys stat sol (a) **137**: 327-335.

[12] Kittler M, Seifert W, Stemmer M, Palm J (1995) Interaction of iron with a grain boundary in boron-doped multicrystalline silicon. J Appl Phys **77**: 3725-3728.

[13] Kittler M, Ulhaq-Bouillet C, Higgs V (1995) Influence of copper contamination on recombination activity of misfit dislocations in SiGe/Si epilayers: Temperature dependence of activity as a marker characterizing the contamination level. J Appl Phys **78**, 4573-4583.

[14] Kittler M, Seifert W, Higgs V (1995) Modification of recombination activity of dislocations in Si and SiGe by contamination and hydrogenation. Proc. Materials Research Society **378** (Symp. B: Defects and Impurity Engineered Semiconductors and Devices; in press).

[15] Knobloch K, Kittler M, Seifert W, Higgs V (1995) Scanning DLTS measurements of extended defects in silicon. In: Proc. Polycrystalline Semiconductors IV - Physics, Chemistry and Technology (POLYSE 1995). Pizzini S, Strunk HP, Werner JH (eds.). To be published in: Solid State Phenomena, Trans. Tech. Publ., Zug, Switzerland (in press).

[16] Leamy HJ (1982) Charge collection scanning electron microscopy. J Appl Phys **53**: R51-R80.

[17] Leamy HJ, Kimerling LC, Ferris SD (1976) Silicon single crystal characterization by SEM. Scanning Electron Microsc **1976**; I: 529-538.

[18] Leamy HJ, Kimerling LC, Ferris SD (1978) Electron beam induced current. Scanning Electron Microsc **1978**; I: 717-725.

[19] Lemke H (1981) Dotierungseigenschaften von Eisen in Silizium (Doping properties of iron in silicon). phys stat sol (a) **64**: 215-224 (in German).

[20] Radzimski ZJ, Zhou TQ, Buczkowski A, Rozgonyi GA, Finn D, Hellwig LG, Ross JA (1992) Recombination at clean and decorated misfit dislocations. Appl Phys Lett **60**: 1096-1098.

[21] Radzimski ZJ, Buczkowski A, Zhou TQ, Dube A, Rozgonyi GA (1993) Electron beam induced current studies of defect induced conductivity inversion. Scanning Microsc **7**: 513-521.

[22] Rozgonyi GA, Kola RR (1989) Defect engineering for ULSI epitaxial silicon. Solid State Phenomena **6&7**: 143-158.

[23] Shimura F (1989) Semiconductor Silicon Crystal Technology. Academic Press, San Diego, CA. pp. 146-171.

[24] Stemmer M (1994) Monte Carlo simulation of the minority-carrier recombination at and around grain boundaries surrounded by a denuded zone revealed by light-beam-induced current mapping. Mater Sci Eng **B24**: 180-183.

[25] Stemmer M, Martinuzzi S, Pasquinelli M (1993) On the interaction of transition metals with silicon grain boundaries. Solid State Phenomena **32&33**: 105-110.

[26] Zoth G, Bergholz W (1990) A fast, preparation-free method to detect iron in silicon. J Appl Phys **67**: 6764-6771.

Discussion with Reviewers

Z.J. Radzimski: Did you try to estimate the energy levels of defects using temperature dependent EBIC results? It would be interesting to figure out whether such results would match well-known levels for FeB and Fe_i defect levels mentioned in the paper.

Authors: The temperature-dependent recombination studies by EBIC allow, frequently, a separation between deep and shallow levels. However, we believe there is no chance to get real spectroscopic information that will allow one to identify an unknown defect level/impurity. That is due to the fact that the temperature dependence of the capture cross-section, $\sigma(T)$, and of other parameters as minority-carrier diffusivity, for example, is not generally available or not sufficiently well known, respectively. So, for material containing interstitial iron (acting as a deep trap), the diffusion length does not weakly increase upon cooling, as it is expected commonly for deep levels, but, on the contrary, was found to decrease strongly [12]. This is a consequence of the strong temperature dependence of $\sigma(Fe_i)$ [19].

A. Cavallini: You emphasized the high sensitivity of EBIC for revealing iron distribution in B-doped Si. Do you believe that this microanalytical application of the EBIC technique could be extended to the investigation of the extrinsic gettering by dislocations? I refer, in particular, to the study of bright haloes around dislocations in Si-doped and Te-doped GaAs.

Authors: We believe that the bright haloes around extended defects reflect the interaction of impurities with the defects in a more or less sensitive manner; for Si, see e.g., ref. [7]; and the work of Frigeri [28, 29] for GaAs, where segregation of dopants around extended defects could be studied for concentration levels above the ppm range. However, to realize by EBIC an ultra-sensitive semi-quantitative analysis of the amount and distribution of gettered atoms in the ppb range, favorable conditions must be fulfilled. This was demonstrated to be the case for Fe in B-doped Si, where one can make use of the very different recombination properties of iron-boron pairs and of interstitial iron. Probably other species of relevance in semiconductor materials exhibiting similar advantages exist, we have to find them out.

Z.J. Radzimski: Could you quantify the effects of phosphorus striations, i.e., the striation contrast for 10 and 40 keV beam energy or the carrier concentration variation expected etc.?

Authors: Unfortunately, we cannot quantify these effects accurately. At 40 keV, the striation-induced contrast is near the detection limit (about 0.5%), but at 10 keV, it amounts to a few percent. A quantification of the variation of carrier concentration is not possible so far for our material (see also the text). However, it must be smaller than the detection limit of the spreading resistance method, which allows to detect a dopant variation of about 10% at a doping level around 10^{14} cm^{-3}. Please refer to the paper by Frigeri [27]: in his material, the bulk diffusion length is very small, so that, under high beam energy conditions, the variation of depletion layer width causes a marked variation of the EBIC signal (much stronger than in our FZ-grown Si) and allows a quantification of the dopant variation.

Reviewer III: Are the results about the striations of practical relevance, i.e. is your FZ-grown Si provided by a commercial supplier?

Authors: The micrographs shown in Figures 7 and 8 were taken from material not grown by a commercial supplier. The samples were cut from an ingot and mirror polished before preparation of the Schottky barrier. However, also in P-doped FZ-grown wafers by Wacker, similar contrasts could be detected.

Z.J. Radzimski: Could you compare EBIC images of low and high Cu contaminated dislocations? Did you see formation of precipitates in the latter case? In such a case, the additional structural defects formed around precipitates could be responsible for the strong contrast.

Authors: The c(T) behavior of low Cu contaminated material is shown in Figures 2a, 2b and 2c. The contrast values are below 10%, and in TEM, no precipitates could be detected [13]. In the high Cu contaminated material, the contrast values are much higher (maximum values up to 75%, see Fig. 2d), and in TEM, Cu silicide precipitate colonies and connected with secondary defects, decorating the misfit dislocations, were found [13]. We believe that the high contrasts are caused by the metal silicide precipitates themselves. Even small $NiSi_2$ particles of 10 nm thickness and about 0.8 μm diameter (without secondary defects) exhibit contrasts up to 40% (!) [7]. This strong recombination activity is related to a band bending/potential barrier at the metal

silicide particles [30].

Additional References

[27] Frigeri C (1987) An EBIC method for the quantitative determination of dopant concentration at striations in LEC GaAs. Inst. Phys. Conf. Ser. **87**, 745-750.

[28] Frigeri C (1989) On the nature of the impurity atmosphere around dislocations in bulk n-type GaAs. In: Materials Science Forum **38-41**. Trans Tech Publications, Switzerland. pp. 1379-1384

[29] Frigeri C, Breitenstein O (1990) Influence of shallow donors on the formation of gettering regions in Cz GaAs. In: Defect Control in Semiconductors. Sumino K (ed.). Elsevier Science Publ., Amsterdam. pp. 685-690.

[30] Kittler M, Seifert W (1995) Analysis of recombination activity of $NiSi_2$ platelets in Si. phys. stat. sol. (a) **150**, 463-470.